

Modeling and validation of a parabolic solar collector with a heat pipe absorber

Kamal A.R. Ismail*, Maurício A. Zanardi^a and Fátima A.M. Lino^b

Faculty of Mechanical Engineering, Department of Energy, State University of Campinas, Mendeleiev street, 200, Cidade Universitária "Zeferino Vaz", Barão Geraldo, Postal Code 13083-860, Campinas, SP, Brazil

(Received January 15, 2016, Revised December 6, 2016, Accepted December 7, 2016)

Abstract. Cylindrical parabolic solar concentrators of small concentration ratio are attractive options for working temperatures around 120°C. The heat gained can be utilized in many applications such as air conditioning, space heating, heating water and many others. These collectors can be easily manufactured and do not need to track the sun continuously. Using a heat pipe as a solar absorber makes the system more compact and easy to install. This study is devoted to modeling a system of cylindrical parabolic solar concentrators of small concentration ratio (around 5) fitted with a heat pipe absorber with a porous wick. The heat pipe is surrounded by evacuated glass tube to reduce thermal losses from the heat pipe. The liquid and vapor flow equations, energy equation, the internal and external boundary conditions were taken into consideration. The system of equations was solved and the numerical results were validated against available experimental and numerical results. The validated heat pipe model was inserted in an evacuated transparent glass tube as the absorber of the cylindrical parabolic collector. A calculation procedure was developed for the system, a computer program was developed and tested and numerical simulations were realized for the whole system. An experimental solar collector of small concentration, fitted with evacuated tube heat pipe absorber was constructed and instrumented. Experiments were realized with the concentrator axis along the E-W direction. Results of the instantaneous efficiency and heat gain were compared with numerical simulations realized under the same conditions and reasonably good agreement was found.

Keywords: parabolic concentrator; concentrator with heat pipe; solar energy; evacuated enveloped heat pipe

1. Introduction

The cylindrical parabolic solar collector is composed of a mirror of cylindrical parabolic geometry with the absorber placed in the focal region of the mirror. The efficiency of the collector is essentially influenced by thermal and optical losses. The optical losses are depending on the mirror fabrication precision and orientation. For a mirror fabricated within acceptable levels of quality, having precise collector orientation and sun tracking, the optical losses will tend to be

*Corresponding author, Professor, E-mail: kamal@fem.unicamp.br

^aPh.D., E-mail: mzanardi@feg.unesp.br

^bPh.D., E-mail: fatimalino@fem.unicamp.br

constant and small. Hence, in order to improve the overall efficiency of the collector system, it is necessary to reduce the thermal losses, which are inherent to the collector itself.

The thermal losses depend upon the temperature of the absorber tube, the thermal conductivity of the tube material and the convective resistance between the working fluid and the tube wall. To reduce the conduction and convection losses, the absorber tube is housed inside an external glass tube having vacuum in the annular gap between the two tubes. Additionally, the radiation losses are reduced by using selective coatings on the absorber surface. The heat exchange between the absorber tube and the working fluid can be improved by enhancing the convection heat transfer coefficient by adequate choice of the working fluid, increasing the fluid Reynolds number, use of techniques for heat transfer augmentation as micro fins, spiral strips, etc.

Working fluids to extract heat from the condensers of the heat pipes vary according to the temperature achieved by the project of the parabolic collector. For temperatures below 100°C water is used. For higher temperatures fluids of higher vaporization temperatures are used. Silicon and Therminol oils are most preferred. For temperatures below 100°C the best storage medium is water. For higher temperatures liquid storage is not as attractive as storage in latent heat which is covering a wide range of working temperatures. PCM storage is usually preferred because of the high storage density and nearly constant temperatures during charging and discharging processes.

One of the advantages of incorporating heat pipes in the absorbing unit of the collector is that the heat removal is accomplished by the external surface of the condenser of the heat pipe which can be improved by the conventional fin technique. Another advantage is that by using heat pipes the necessary pumping power is reduced.

Ortobasi and Buehl (1980) presented an optical and experimental study on a tubular solar collector with a heat pipe absorber. Vasiliev, Grakovich *et al.* (1984) developed a model for flat plate solar collector with heat pipes and demonstrated that the use of the heat pipes can improve the efficiency by 10 to 17%. Azad, Bahar *et al.* (1987) reported the results of an experimental and numerical study on solar water heaters using gravity assisted methanol heat pipes.

Gari and Fathalah (1988) presented a model simulation and experimental results of a passive condensate heat pipe pumping system using acetone as a working fluid. Ismail and Zanardi (1990) presented a numerical and experimental study on solar concentrators of small concentration ratio equipped with heat pipes, analyzed the optical and thermal losses of the system and validated their model with experimental data.

Azad and Bahar (1991) analyzed the coaxial heat pipe solar collector and compared the numerical predictions with experimental results. Ghaddar and Nasr (1998) presented the results of an experimental study on heat pipe solar collector with R11 as a working fluid, while Chun, Kang *et al.* (1999) presented an experimental study for the utilization of heat pipes for domestic solar water heaters. Hussein, Mohamad *et al.* (1999) presented the results of optimization of a wickless heat pipe flat plate solar collector by using a transient thermal model for the solar system.

Kim and Seo (2007) numerically and experimentally investigated the thermal performance of a glass evacuated tube solar collector consisting of a two layered glass tube and an absorber tube. Air was used as the working fluid. The length and diameter of this glass tube were 1200 and 37 mm, respectively. Four different shapes of absorber tubes were considered, and the performances of the solar collectors were studied to find the best shape of the absorber tube for the solar collector. Beam irradiation, diffuse irradiation, and shade due to adjacent tubes are taken into account for a collector model to obtain a realistic estimation.

Redpath, Eames *et al.* (2009) presented experimental data from a heat pipe evacuated tube solar water heater. The high capital costs associated with heat pipe evacuated tube solar water heating

systems can be reduced by replacing forced circulation with thermosyphon circulation.

Kumar and Reddy (2009) presented a three dimensional numerical analysis of the porous disc line receiver for solar parabolic trough collector. The influence of thermal fluid properties, receiver design and solar radiation concentration on the overall heat collection is investigated. The analysis is carried out based on renormalization-group (RNG) k - ϵ turbulent model and Therminol-VP1 as working fluid. The use of porous medium in tubular solar receiver enhances the system performance significantly.

Padilla, Demirkaya *et al.* (2011) performed a detailed one dimensional numerical heat transfer analysis of a solar parabolic trough collector. The receiver and envelope were divided into several segments and mass and energy balances were applied in each segment. The partial differential equations were solved simultaneously. Finally, the numerical results were validated against experimental data from Sandia National Laboratory (SNL) and models showing good agreement with experimental data.

Nkwetta, Smyth *et al.* (2012) presented the performance of an evacuated tube heat pipe solar collector compared to a concentrated evacuated tube single-sided coated heat pipe absorber for medium temperature applications. The concentrated evacuated tube heat pipe solar collector showed an improvement of 30% and 25.42% in overall average temperature gain and total daily collected energy, respectively compared to the non-concentrated evacuated tube heat pipe collectors.

Chong, Chay *et al.* (2012) proposed a cost effective easy fabricated V-trough solar water heater system using forced circulation system. Integrating the solar absorber with the easily fabricated V-trough reflector can improve the performance of solar water heater system. They realized optical analysis, experimental study and cost analysis of the stationary V-trough solar water heater system and reported promising results in both optical efficiency of V-trough reflector and the overall thermal performance of the solar water heater.

Parabolic trough solar collector is the most proven industry scale solar generation technology today available. The thermal performance of such devices is of major interest for optimizing the solar field output and increase the efficiency of power plants. Hachicha, Rodríguez *et al.* (2013) presented a detailed numerical heat transfer model based on the finite volume method for these equipment where the different elements of the receiver were discretized into several segments in both axial and azimuth directions and energy balances were applied for each control volume. An optical model was also developed for calculating the non-uniform solar flux distribution around the receiver. The model was thoroughly validated with results from the literature. In all cases, results obtained showed a good agreement with experimental and analytical results.

Arab and Abbas (2013) developed a semi-dynamic model of a concentric evacuated tube solar water heater to investigate the effect of working fluid choice on the technical and economic performance of a typical solar water heater and validated the numerical predictions against experimental data. The effects of using water, ammonia, acetone, methanol, and pentane as working fluids of the built-in heat pipe were discussed. They reported that the performance of the solar water heater can be significantly enhanced up to 28% and 50% from economical and technical points of view, respectively.

Ayompe and Duffy (2013) presented the results and analysis of the thermal performance of a solar water heating system with heat pipe evacuated tube collector using data obtained from one year field testing. They reported solar collector efficiency of about 63.2% and system efficiency of about 52.0%.

Cabrera, Fernandez-Garcia *et al.* (2013) summarized the existing experiences and realizations

on applications of parabolic trough collectors in solar cooling systems, presented a survey of the new collectors with potential application in feeding absorption chillers and evaluated its occasional use as an alternative to other solar thermal collectors. They reported that parabolic trough collectors present similar leveled costs of energy for cooling as flat plate collector and lower than evacuated tube collectors and compound parabolic collectors.

Wang, Zhu *et al.* (2015) developed and studied a tracking compound parabolic concentrating solar collector with concentration ratio of 2.3, which combine the compound parabolic concentrating, heat pipe evacuated tubular receiver and crank rod transmission mechanism together. A theoretical model was created to simulate the solar incident angles and the optical performance of the tracking compound parabolic concentrating collector. In addition, thermal performance of the tracking compound parabolic concentrating collector at different operation modes was investigated experimentally.

Liang, You *et al.* (2015) summarized the one dimensional mathematical models under different assumptions and details for parabolic trough solar collectors. All the heat transfer processes were considered: convection within the absorber, in the annulus and between the glass and ambient; conduction through glass cover, absorber and support brackets; radiation in the annulus and from the glass to the sky. The difference in accuracy for one dimensional model was presented and analyzed on the basis of the experimental data from Sandia National Laboratories. The average difference of outlet temperature between the simulation results and test data was 0.65°C , however it was 2.69°C between the 3-D model and experiment results.

Biencinto, González *et al.* (2016) described and evaluated a new simulation model for direct steam generation in parabolic trough solar collectors. The model is based on a steady state approach but deals with transient conditions such as start-up, shutdown and clouds in a reasonable computing time. The performance of the model is validated with real experimental data.

Jebasingh and Herbert (2016) presented a review paper focused on the performance and efficiency of solar parabolic trough collector and also reviewed the pertinent applications of solar energy such as air heating system, desalination, refrigeration, industrial heating purposes and power plants.

In cold environment, the conventional flat plate solar collectors and all glass evacuated tube solar collectors will suffer from various problems, such as large heat loss, low efficiency, freeze and tube burst, which severely limit their applications. For this reason Zou, Dong *et al.* (2016) proposed for water heating in cold areas a special small size parabolic trough solar collector, which could overcome the shortcomings of conventional solar collectors. An experimental platform was developed, and extensive tests were conducted to evaluate the characteristics of the proposed parabolic trough solar collector. It was found that the thermal efficiency of the proposed parabolic trough solar collector reached about 67% even under the condition of solar radiation of less than 310 W/m^2 , indicating that the parabolic trough solar collector could collect solar radiation efficiently. The results showed that the efficiency increased with the increase of the output temperature, and was reduced by wind action and frosting.

Guo, Huai *et al.* (2016) investigated the influences of some parameters on the performance of parabolic trough solar receiver such as the mass flow rate of working fluid, ambient temperature and solar incident angle on the heat losses of solar receiver. The exergy losses of solar receiver increase as the inlet temperature of working fluid, wind velocity, and the inner diameter of glass cover increase. The convective heat loss of glass cover predominates in the heat losses of solar receiver, but the exergy lost from absorber ends takes the largest proportion. The optical heat loss of solar collector is far more than the heat losses of solar receiver. There exists an optimal mass flow rate of working fluid for exergy efficiency.

Conrado, Rodriguez-Pulido *et al.* (2017) presented an up-to-date review on the thermal performance of parabolic trough solar collectors. Various types of mathematical models, simulation and numerical methods, and experimental set-ups of the parabolic trough solar collectors were reviewed and analyzed in terms of heat loss, environmental conditions, temperature and heat flux. Furthermore, they reported cost analysis and economic strategy used for the parabolic trough solar collector collectors.

Considering the above literature revision, this paper presents a complete model for a cylindrical parabolic solar concentrator of low concentration ratio fitted with heat pipe absorber. A detailed model of the heat pipe with porous wick is developed, solved numerically by the finite volume method. The grid size was optimized and the numerical predictions were compared with well accepted experimental results. A model for the trough parabolic solar collector with the porous heat pipe enveloped in evacuated glass tube is used as a heat absorber was developed. The available formulations and data on the optical and thermal losses were incorporated in the model. The numerical predictions of the system composed of the collector and the porous wicked heat pipe were compared with experimental results to validate the model and the numerical simulations with the system oriented along the E-W direction. Reasonably good agreement was found.

2. The mathematical model

2.1 The heat pipe full model

Fig. 1 shows a heat pipe of circular cross section used as an absorber for the solar concentrator. In order to formulate the heat pipe mathematical model some assumptions are made to facilitate the mathematical treatment (Chi 1976). These assumptions include that the liquid and vapor flow in the heat pipe is laminar, steady; the vapor flow is subsonic and that the thermo-physical properties of the liquid and vapor are constant in the temperature range of operation of the heat pipe. Although this last condition is used in the present study, the model developed allows for the variation of the physical properties with temperature. Also it is assumed that the vapor fills the interior of the tube, the processes of condensation and evaporation occurs at the liquid-vapor interface which coincides with the physical interface between the porous wick and the vapor region. Finally it is assumed that at the vapor-liquid interface, the vapor is in a state of thermodynamic equilibrium corresponding to the local pressure.

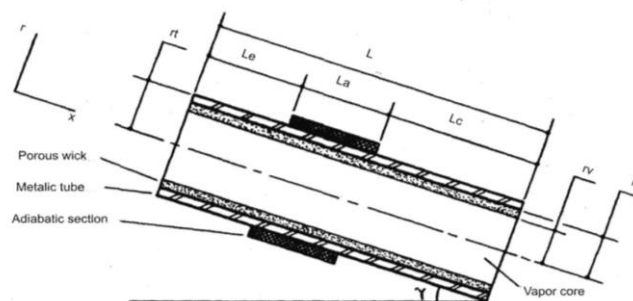


Fig. 1 Heat pipe schematic representation

Using the above assumptions and the geometry presented in Fig. 1, the liquid flow in the porous structure is formulated based on the equations developed by Vafai and Tien (1981) in its conservative form. Hence the equation of mass conservation, equation of momentum in the x-direction, equation of momentum in the r-direction and equation of energy were written in their conservative forms (not shown here to avoid excessive and repeated equations). In these equations the effective thermal conductivity, k_{eff} of the porous saturated medium and its permeability K are used to define the porous material of the heat pipe wick structure.

The vapor flow in the heat pipe flows in the in the core of the tube and is described by the Navier Stokes equations together with the equations of continuity and equation of energy written in their conservative forms, that is, the equation of mass conservation, equation of momentum in the x-direction, equation of momentum in the r-direction and equation of energy were written in their conservative forms (not shown here to avoid excessive and repeated equations).

The heat transfer in the metallic tube is governed by the steady state heat conduction equation. In order to facilitate the numerical treatment of these equations we adopted the dimensionless variables presented below

$$x^* = \frac{x}{L}; \quad r^* = \frac{r}{r_v}; \quad u^* = \frac{u}{v_r}; \quad v^* = \frac{v}{v_r}; \quad \rho^* = \frac{\rho}{\rho_r}; \quad \mu^* = \frac{\mu}{\mu_r}; \quad p^* = \frac{p}{\rho_r v_r^2} \quad (1)$$

$$v_r = \frac{Q}{2\pi r_v L_e \rho_v \lambda}$$

Where v_r is a reference velocity related to the energy rate Q by the equation

While ρ_r and μ_r are respectively the reference density and reference viscosity in a given temperature and λ is the latent heat of vaporization of the heat pipe working fluid. For constant properties $\rho^* = \mu^* = 1$

These dimensionless variables are also used to calculate the dimensionless numbers such as Re_r , Pr , D_{ar} and others as below

$$Re_r = \frac{\rho_{vr} v_r r_r}{\mu_{vr}}; \quad Pr = \frac{\mu_{vr} c_{pv}}{k_v}; \quad Re_{rp} = \frac{\mu_{vr} \rho_{lr}}{\mu_{lr} \rho_{vr}} \quad (2)$$

$$Pr_p = \frac{\mu_{lr} c_{pl}}{k_{eff}}; \quad D_{ar} = \frac{r_v^2 \varepsilon}{K}$$

Where D_{ar} is the Darcy's number. It is important to mention that the boundary conditions for the governing equations are not commented at this stage but will be presented in their dimensionless forms together with the governing equations. The above dimensionless variables listed above were substituted in the governing equations (described in their conservative form) to obtain the system of equations and their associated boundary conditions as below:

The liquid phase

- Mass conservation equation

$$\frac{r_v}{L} \frac{\partial}{\partial x^*} \left(\frac{\rho_l^* r^{*n} u_l^*}{\varepsilon} \right) + \frac{\partial}{\partial r^*} \left(\frac{\rho_l^* r^{*n} v_l^*}{\varepsilon} \right) = 0 \quad (3)$$

- Flow equation in the x-direction

$$\begin{aligned}
 & \frac{1}{r^*} \left\{ \frac{r_v}{L} \frac{\partial}{\partial x^*} \left(\frac{\rho_l^* r^* u_l^*}{\varepsilon} \right) u_l^* + \frac{\partial}{\partial r^*} \left(\frac{\rho_l^* r^* v_l^*}{\varepsilon} \right) u_l^* - u_l^* \left[\frac{r_v}{L} \frac{\partial}{\partial x^*} \left(\frac{\rho_l^* r^* u_l^*}{\varepsilon} \right) + \frac{\partial}{\partial r^*} \left(\frac{\rho_l^* r^* v_l^*}{\varepsilon} \right) \right] \right\} \\
 &= - \left(\frac{r_v}{L} \right) \frac{\partial p_l^*}{\partial x^*} + \frac{1}{r^*} \left\{ \left(\frac{r_v}{L} \right)^2 \frac{1}{Re_{rp}} \frac{\partial}{\partial x^*} \left(\frac{\mu_l^* r^* \frac{\partial u_l^*}{\partial x^*}}{\varepsilon} \right) + \frac{1}{Re_{rp}} \frac{\partial}{\partial r^*} \left(\frac{\mu_l^* r^* \frac{\partial u_l^*}{\partial r^*}}{\varepsilon} \right) \right\} \\
 & - \frac{Dar}{Re_{rp}} \mu_l^* u_l^* + \frac{\rho_l^* r_v}{\varepsilon v_r} g \sin \gamma
 \end{aligned} \tag{4}$$

- Flow equation in the radial-direction

$$\begin{aligned}
 & \frac{1}{r^*} \left\{ \frac{r_v}{L} \frac{\partial}{\partial x^*} \left(\frac{\rho_l^* r^* u_l^*}{\varepsilon} \right) v_l^* + \frac{\partial}{\partial r^*} \left(\frac{\rho_l^* r^* v_l^*}{\varepsilon} \right) v_l^* - v_l^* \left[\frac{\partial}{\partial x^*} \left(\frac{\rho_l^* r^* u_l^*}{\varepsilon} \right) + \frac{\partial}{\partial r^*} \left(\frac{\rho_l^* r^* v_l^*}{\varepsilon} \right) \right] \right\} \\
 &= - \frac{\partial p_l^*}{\partial r^*} + \frac{1}{r^*} \left\{ \left(\frac{r_v}{L} \right)^2 \frac{1}{Re_{rp}} \frac{\partial}{\partial x^*} \left(\frac{\mu_l^* r^* \frac{\partial v_l^*}{\partial x^*}}{\varepsilon} \right) + \frac{1}{Re_{rp}} \frac{\partial}{\partial r^*} \left(\frac{\mu_l^* r^* \frac{\partial v_l^*}{\partial r^*}}{\varepsilon} \right) \right\} \\
 & - \frac{Dar}{Re_{rp}} \mu_l^* v_l^* - \frac{1}{Re_{rp}} \frac{\mu_l^* r^* v_l^*}{r^{*2}}
 \end{aligned} \tag{5}$$

- Energy equation

$$\begin{aligned}
 & \frac{1}{r^{*n}} \left\{ \frac{r_v}{L} \frac{\partial}{\partial x^*} \left(\frac{\rho_l^* r^{*n} u_l^*}{\varepsilon} \right) T_l + \frac{\partial}{\partial r^*} \left(\frac{\rho_l^* r^{*n} v_l^*}{\varepsilon} \right) T_l - T_l \left[\frac{r_v}{L} \frac{\partial}{\partial x^*} \left(\frac{\rho_l^* r^{*n} u_l^*}{\varepsilon} \right) + \frac{\partial}{\partial r^*} \left(\frac{\rho_l^* r^{*n} v_l^*}{\varepsilon} \right) \right] \right\} \\
 &= \frac{1}{r^{*n}} \left\{ \left(\frac{r_v}{L} \right)^2 \frac{\partial}{\partial x^*} \left(\frac{\mu_l^* r^{*n} \frac{\partial T_l}{\partial x^*}}{Re_{rp} Pr_p} \right) + \frac{1}{Re_{rp}} \frac{\partial}{\partial r^*} \left(\frac{\mu_l^* r^{*n} \frac{\partial T_l}{\partial r^*}}{Re_{rp} Pr_p} \right) \right\}
 \end{aligned} \tag{6}$$

The vapor phase

- Mass conservation equation

$$\frac{r_v}{L} \frac{\partial}{\partial x^*} (\rho_v^* r^{*n} u_v^*) + \frac{\partial}{\partial r^*} (\rho_v^* r^{*n} v_v^*) = 0 \tag{7}$$

- Flow equation in the x-direction

$$\frac{1}{r^{*n}} \left\{ \frac{r_v}{L} \frac{\partial}{\partial x^*} (\rho_v^* r^{*n} u_v^*) \mu_v^* + \frac{\partial}{\partial r^*} (\rho_v^* r^{*n} v_v^*) \mu_v^* - u_v^* \left[\frac{\partial}{\partial x^*} (\rho_v^* r^{*n} u_v^*) + \frac{\partial}{\partial r^*} (\rho_v^* r^{*n} v_v^*) \right] \right\}$$

$$= -\left(\frac{r_v}{L}\right) \frac{\partial \hat{p}_v^*}{\partial x^*} + \frac{1}{r^{*n}} \left\{ \left(\frac{r_v}{L}\right)^2 \frac{1}{Re_r} \frac{\partial}{\partial x^*} \left(\mu_v^* r^{*n} \frac{\partial u_v^*}{\partial x^*} \right) + \frac{1}{Re_r} \frac{\partial}{\partial r^*} \left(\mu_v^* r^{*n} \frac{\partial u_v^*}{\partial r^*} \right) \right\} + \rho_v^* \frac{r_v}{v_r} g \text{seny} \quad (8)$$

- Flow equation in the radial-direction

$$\begin{aligned} & \frac{1}{r^{*n}} \left\{ \frac{r_v}{L} \frac{\partial}{\partial x^*} \left(\rho_v^* r^{*n} u_v^* \right) + \frac{\partial}{\partial r^*} \left(\rho_v^* r^{*n} v_v^* \right) \right\} - v_v^* \left[\frac{r_v}{L} \frac{\partial}{\partial x^*} \left(\rho_v^* r^{*n} u_v^* \right) + \frac{\partial}{\partial r^*} \left(\rho_v^* r^{*n} v_v^* \right) \right] \\ & = -\frac{\hat{q}_v^*}{\partial r^*} + \frac{1}{r^{*n}} \left\{ \left(\frac{r_v}{L}\right)^2 \frac{1}{Re_r} \frac{\partial}{\partial x^*} \left(\mu_v^* r^{*n} \frac{\partial v_{vl}^*}{\partial x^*} \right) + \frac{1}{Re_r} \frac{\partial}{\partial r^*} \left(\mu_v^* r^{*n} \frac{\partial v_v^*}{\partial r^*} \right) \right\} - n \frac{1}{Re_r} \frac{\mu_v^* r^{*n} v_v^*}{r^{*2n}} \end{aligned} \quad (9)$$

- Energy equation

$$\begin{aligned} & \frac{1}{r^*} \left\{ \frac{r_v}{L} \frac{\partial}{\partial x^*} \left(\rho_v^* r^{*n} u_v^* \right) T_v + \frac{\partial}{\partial r^*} \left(\rho_v^* r^{*n} v_v^* \right) T_v - T_v \left[\frac{r_v}{L} \frac{\partial}{\partial x^*} \left(\rho_v^* r^{*n} u_v^* \right) + \frac{\partial}{\partial r^*} \left(\rho_v^* r^{*n} v_v^* \right) \right] \right\} \\ & = \frac{1}{r^*} \left\{ \left(\frac{r_v}{L}\right)^2 \frac{\partial}{\partial x^*} \left(\frac{\mu_l^*}{Re_r Pr} r^* \frac{\partial T_v}{\partial x^*} \right) + \frac{\partial}{\partial r^*} \left(\frac{\mu_v^*}{Re_r Pr} r^* \frac{\partial T_v}{\partial r^*} \right) \right\} \end{aligned} \quad (10)$$

- The heat conduction equation for the metallic shell of the tube is

$$\left(\frac{r_v}{L}\right)^2 \frac{\partial}{\partial x^*} \left(k_m \frac{\partial T_m}{\partial x^*} \right) + \frac{\partial}{\partial r^*} \left(k_m \frac{\partial T_m}{\partial r^*} \right) = 0 \quad (11)$$

The boundary conditions for this problem are divided into two sets, boundary conditions far from the interface and boundary conditions at the interface.

Boundary conditions far from the interface

For the vapor flow

- No slip at the solid surface

$$v_v^*(0, r^*) = v_v^*(1, r^*) = 0 \quad (12a)$$

- Solid lateral walls

$$u_v^*(0, r^*) = u_v^*(1, r^*) = 0 \quad (12b)$$

- Symmetry with respect to $r=0$

$$v_v^*(x^*, 0) = 0; \quad \frac{\partial u_v^*}{\partial r^*}(x^*, 0) = 0; \quad \frac{\partial T_v^*}{\partial r^*}(x^*, 0) = 0 \quad (12c)$$

- Insulated lateral walls

$$\frac{\partial T_v^*}{\partial x^*}(0, r^*) = 0; \quad \frac{\partial T_v^*}{\partial x^*}(1, r^*) = 0 \quad (12d)$$

For the liquid flow

- No slip on the solid surfaces

$$v_l^*(0, r^*) = v_l^*(1, r^*) = 0 \quad (13a)$$

- Lateral solid walls

$$u_l^*(0, r^*) = u_l^*(1, r^*) = 0 \quad (13b)$$

- Insulated lateral walls

$$\frac{\partial T_l^*}{\partial x^*}(0, r^*) = 0; \quad \frac{\partial T_l^*}{\partial x^*}(1, r^*) = 0 \quad (13c)$$

- Insulated lateral walls

$$\frac{\partial T_m^*}{\partial x^*}(0, r^*) = 0 \quad (14a)$$

$$\frac{\partial T_m^*}{\partial x^*}(1, r^*) = 0 \quad (14b)$$

- Heat flux in the evaporator and condenser

$$\frac{-k_m}{L} \frac{\partial T_m^*}{\partial x^*}(x^*, \frac{r_l}{L}) = \pm \frac{Q}{2\pi r_l L_e} \quad (14c)$$

In Eq. (14c) the (\pm) signs refer to the condenser and evaporator respectively. This condition can be changed according to the way heat is removed from the condenser.

Boundary conditions at the interface

Liquid-vapor interface

- Energy balance at the interface

$$v_v^*(x^*, 1) = \frac{1}{v_r} \left\{ \left[\frac{-k_{eff}}{\rho_{vr} r_v} \frac{\partial T_l}{\partial r^*} + \frac{k_v}{\rho_{vr} r_v} \frac{\partial T_v}{\partial r^*} \right] (\rho^* \lambda)^{-1} \right\} \quad (15a)$$

- Mass conservation at the interface

$$v_l^*(x^*, 1) = \frac{\rho_{vr}\rho_v^*}{\rho_{lr}\rho_l^*} v_v^*(x^*, 1) \quad (15b)$$

- Continuity of the velocity at the interface

$$u_v^*(x^*, 1) = u_l^*(x^*, 1) \quad (15c)$$

- Equal shear stress at the interface

$$\frac{\partial v_v^*}{\partial r^*}(x^*, 1) = \frac{\mu_{lr}\mu_l^*}{\mu_{vr}\mu_v^*} \frac{\partial v_l^*}{\partial r^*}(x^*, 1) \quad (15d)$$

- Liquid-vapor equilibrium

$$T_v(x^*, 1) = T(p) \quad (15e)$$

- Temperature continuity at the interface

$$T_v(x^*, 1) = T_l(x^*, 1) \quad (15f)$$

At the liquid-metallic tube interface

- Solid wall

$$v_l^*\left(x^*, \frac{r_p}{r_v}\right) = 0 \quad (16a)$$

- No slip at the solid surface

$$u_l^*\left(x^*, \frac{r_p}{r_v}\right) = 0 \quad (16b)$$

- Continuity of the heat flux at the interface

$$k_m \frac{\partial T_m}{\partial r^*}\left(x^*, \frac{r_p}{r_v}\right) = k_{eff} \frac{\partial T_l}{\partial r^*}\left(x^*, \frac{r_p}{r_v}\right) \quad (16c)$$

- Continuity of the temperature at the interface

$$T_m\left(x^*, \frac{r_p}{r_v}\right) = T_l\left(x^*, \frac{r_p}{r_v}\right) \quad (16d)$$

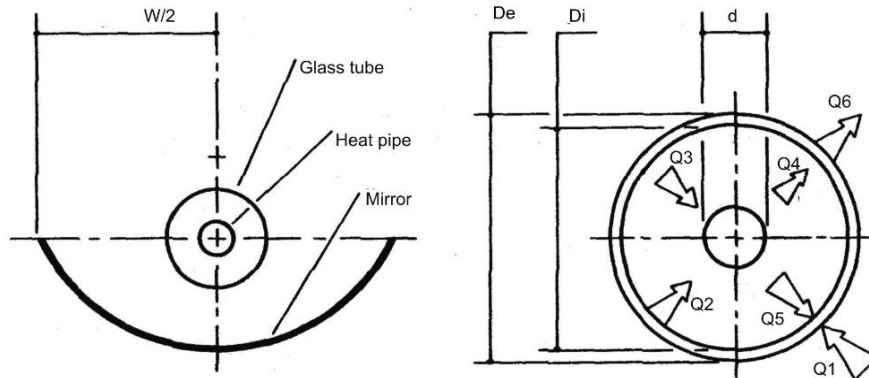


Fig. 2 Geometry of the parabolic concentrator

To solve the system of coupled equations subject to the associated boundary conditions, the authors used the finite volume method, the Locally Analytical Differencing Scheme (LOAD) proposed by Wong and Raithby (1979). Extensive number of numerical tests was realized and the details were omitted here for brevity.

2.2 The solar collector model

Fig. 2 shows a section across the parabolic trough solar collector. The glass parabolic mirror has a width W . The porous black painted heat pipe has an external diameter d surrounded by the glass evacuated tube of external diameter D_e and internal diameter D_i . A section across the absorber tube is shown on the left side of Fig. 2 indicating the fluxes of radiation and heat received by and emitted from the absorber porous heat pipe. The mathematical model is formulated based upon the collector geometry shown in Fig. 2.

The following simplifying assumptions are considered:

- The system is in thermal equilibrium.
- The solar beams are parallel.
- The optical properties are constant over the spectrum used and do not depend on the temperature, the angle of incidence or polarization.
- The evaporator of the heat pipe and the glass tube have uniform circumferential temperature because of the low concentration ratio of the collector.

The radiation heat transfer contributions considered include two sources, one is the solar radiation including the visible and infrared ranges, while the other is the heat exchange in the infrared range corresponding to the absorber temperature. The optical properties are considered constant in the respective radiation ranges.

2.3 Solar radiation

Based upon Fig. 2, and considering a section of the absorber tube of length Δz it is possible to write the following equations:

- The flux of solar energy striking the external glass tube directly or after reflection from the mirror is

$$Q_1 = E \rho_e (W - D_e) Y_{tv} \Delta z + E(D_i - d) \Delta z + E d \Delta z + E(D_i - d) \tau_{vv}^2 \rho_e Y_{tv} \Delta z \quad (17)$$

- The flux of energy emitted from the internal surface of the glass tube is

$$Q_2 = \tau_{vv} Q_1 + \rho_{vv} Q_5 \quad (18)$$

- The flux of energy reaching the absorber is

$$Q_3 = \tau_{vv} \rho_e E(W - D_e) Y_{tc} \Delta z + E(D_i - d) \tau_{vv}^3 Y_{tc} \Delta z + \tau_{vv} E d \Delta z + \rho_{vv} Q_5 \left(\frac{d}{D_i} \right) \quad (19)$$

- The flux of energy reflected from the absorber is

$$Q_4 = \rho_{tv} Q_3 \quad (20)$$

- The flux of energy striking the internal surface of the glass tube is

$$Q_5 = Q_4 + \tau_{vv} E \rho_e (W - D_e) Y_{tv} \left(1 - \frac{Y_{tc}}{Y_{tv}} \right) \Delta z + E(D_i - d) \tau_{vv}^3 Y_{tv} \rho_e \left(1 - \frac{Y_{tc}}{Y_{tv}} \right) \Delta z + \\ + E(D_i - d) \tau_{vv} (1 - \tau_{vv}) \Delta z + \rho_{vv} Q_5 \left(1 - \frac{d}{D_i} \right) \quad (21)$$

- The flux of energy lost from the glass tube is

$$Q_6 = \rho_{vv} Q_1 + \tau_{vv} Q_5 \quad (22)$$

In these equations E is given by $E = I F(\alpha) F(\varepsilon)$ and I is the intensity of the solar radiation, $F(\alpha)$ is a correction factor to account for the inclination between the normal to the aperture plane of the solar collector and the solar beam (Duffie and Beckman 2013), and $F(\varepsilon)$ is a function to account for the error in the collector orientation (Duffie and Beckman 2013). The parameters Y_{tv} and Y_{tc} are the interception factors for the glass tube (tv) and the heat pipe (tc) and ρ_{vv} and ρ_{tv} are the reflectance of the glass tube and the absorber respectively.

The inclination of the solar beams to the normal to the aperture area of the collector reduces the aperture area and consequently reduces the reflector surface area due to shading over the reflector.

Following Ramsey, Gupta *et al.* (1977), the function $F(\alpha)$ can be expressed as

$$F(\alpha) = (1 - A) \cos(\alpha)$$

Where A is a function representing the ineffective fraction of the area due to shading.

The function $F(\varepsilon)$ was investigated by Umarov, Zakhidov *et al.* (1976), and their results were used in the present study.

The angle of incidence θ is given by Duffie and Beckman (2013)

$$\cos \theta = \sin \delta \sin \phi \cos s - \sin \delta \cos \phi \cos s \cos \gamma + \cos \delta \cos \phi \cos s \cos \omega + \\ \cos \delta \sin s \cos \gamma \sin \omega + \cos \delta \sin \phi \sin s \cos \gamma \cos \omega$$

Where δ is the sun declination given the approximate equation (Duffie and Beckman, 2013), as

$$\delta = 23.45 \sin \left[360 \frac{(284 + n)}{365} \right]$$

Where n is the day of the year, ϕ is the latitude, s is the angle of inclination between the horizontal plane and the aperture plane, γ is the azimuth of the surface and ω is the hourly angle.

The angles α and ε can be found as function of θ , ω , the solar azimuth γ_s and the solar height β , (Duffie and Beckman 2013).

2.4 Thermal radiation between the absorber and the glass tube

Consider a section of the absorber tube of length Δz as in Fig. 3 and assuming that the metallic tube is at a uniform temperature T_{te} and that the glass tube is at a uniform temperature T_{vi} , the net thermal radiation received by the glass tube and the metallic one can be written as

$$H_v = \frac{\frac{d}{D_i} \varepsilon_v \sigma T_{te}^4 + \varepsilon_v \sigma T_{vi}^4 \left[1 - (1 - \rho_{ti}) \frac{d}{D_i} \right]}{1 - \rho_{vi} \left[1 - (1 - \rho_{ti}) \frac{d}{D_i} \right]} \quad (23)$$

$$\left. \begin{aligned} H_t &= \frac{\varepsilon_v \sigma T_{vi}^4 + \rho_{vi} \varepsilon_t \sigma T_{te}^4 \frac{d}{D_i}}{1 - \rho_{vi} \left[1 - (1 - \rho_{ti}) \frac{d}{D_i} \right]} \\ B_v &= H_t \\ B_t &= \varepsilon_t \sigma T_{te}^4 + \rho_{ti} B_v \end{aligned} \right\} \quad (24)$$

Where ε_t and ε_v are the emittances of the absorber and the glass tube respectively, ρ_{ti} and ρ_{vi} are the respective reflectances.

2.5 Heat transfer by conduction and convection between the glass tube and the absorber

For a horizontal tube of uniform surface temperature surrounded by a second tube of lower surface temperature, with the annular gap filled with air, the total heat loss by conduction and convection can be expressed in the form

$$Q_{cc} = 2\pi k_{ef} \frac{(T_{te} - T_{vi}) \Delta z}{\ln\left(\frac{D_i}{d}\right)} \quad (25)$$

Where k_{ef} , according to Ratzel, Hickox *et al.* (1979), can be given by

$$k_{ef} = k_a \quad \text{for } Ra \leq 1000 \quad (25a)$$

$$k_{ef} = 0.1585 k_a Ra^{0.2667} \quad \text{for } Ra > 1000$$

Where the Rayleigh number R_a may be viewed as the ratio of buoyancy and viscosity forces multiplied by the ratio of momentum and thermal diffusivities and is given by

$$R_a = \rho g \beta l^3 \frac{\Delta T}{\mu \alpha} \quad (25b)$$

$$\Delta T = (T_{te} - T_{vi}) \quad (25c)$$

$$l = \frac{D_i - d}{2} \quad (25d)$$

$$\alpha = \frac{k}{\rho c_p} \quad (25e)$$

The properties ρ , β , μ , α and k_a are expressed in terms of the temperature as in Ratzel, Hickox *et al.* (1979).

2.6 Heat loss by convection to the ambient

The heat loss by convection to the ambient can be expressed as

$$Q_{ca} = \pi D_e h_v (T_{ve} - T_a) \Delta z \quad (26)$$

Where T_{ve} is the temperature of the external surface of the glass tube and T_a is the ambient temperature. The film heat transfer coefficient is given by Kreith, Manglik *et al.* (2011)

$$h_v = 1.41 |T_{ve} - T_a| D_e^{0.25} \quad (27)$$

If the external air velocity along the tube is zero. Alternatively, h_v can be expressed as

$$h_v = k_a C Re^p D_e^{-1} \quad (28)$$

With Re the Reynolds number, C and p are constants depending upon the Reynolds number, k_a , ν and v_a are the thermal conductivity, kinematic viscosity and velocity of air, respectively.

2.7 Heat conduction across the wall of the glass tube

Finally the heat conduction across the wall of the glass tube can be calculated from

$$Q_{ctv} = 2\pi k_v \frac{(T_{vi} - T_{ve})}{\ln\left(\frac{D_e}{D_i}\right)} \Delta z \quad (29)$$

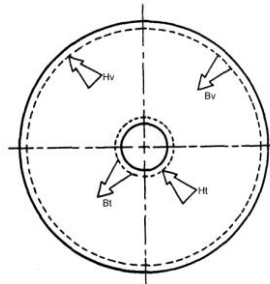


Fig. 3 Thermal radiation exchange between the absorber and the glass tube

2.8 Energy balance

The equations listed above are used to write the energy balance equations for the different elements.

- Energy balance of the absorber

$$Q_u = Q_3 - Q_4 - Q_1^* - Q_{cc} \quad (30)$$

Where Q_u is the useful energy removed by the heat pipe and

$$Q_1^* = \pi d (B_t - H_t) \Delta z$$

- Energy balance of the glass tube as in Fig. 3

$$Q_1 + Q_5 + Q_{cc} + Q_2^* = Q_2 + Q_6 + Q_{ca} + Q_3^* \quad (31)$$

Where

$$Q_2^* = \pi D_i (B_v - H_v) \Delta z$$

And

$$Q_3^* = \pi D_e \sigma \varepsilon_v (T_{ve}^4 - T_a^4) \Delta z + \tau_{vi} Q_2^*$$

- Heat conduction through the glass tube

$$(1 - \tau_{vi}) Q_2^* + Q_{cc} + (1 - \rho_{vv} - \tau_{vv}) Q_5 = Q_{ctv} \quad (32)$$

The three balance equations contain four unknowns, T_{te} , T_{vi} , T_{ve} and Q_u . To determine the four unknowns an additional equation is required to be able to solve the system of equations. The additional equation can be obtained from the analysis of the heat pipe. The determination of the temperature distribution over the heat pipe is done by using the detailed calculation procedure described in Ismail and Zanardi (1993). In this procedure, the determination of the temperature distribution is realized by solving the system of equations for the internal flow in the heat pipe coupled with the energy equations of the vapor and liquid flow and in the wick of the heat pipe.

As the heat removal is realized by circulating a fluid external to the condenser of the heat pipe, the boundary condition can be written in the form

$$-k_m \left. \frac{\partial T_m}{\partial r} \right|_{r=r_t} = h_{cf} [T_t - T_f(x)] \quad (33)$$

And the fluid temperature is determined from

$$\frac{\partial T_f}{\partial x} - \frac{h_{cf} P}{\dot{m} C_p} (T_m - T_f) = 0 \quad (34)$$

Where k_m is the thermal conductivity of the heat pipe material, P is the pipe perimeter, \dot{m} is the mass flow rate in the condenser, ρ and C_p are the density and the specific heat of the fluid. The film heat transfer coefficient h_{cf} can be calculate suggested by Mc Adams (1954)

$$\frac{h_{fc} d}{k_f} = (0.35 + 0.56 Re^{0.52}) Pr^{0.3}$$

3. Procedure for the numerical calculations

The calculation of the temperatures and the useful energy is done following the calculation sequence below.

(i) Using the global formulation for the heat pipe it is possible to write

$$Q_u = A_p U_{hp} (T_{te} - T_{tc}) \quad (35)$$

Where T_{tc} and T_{te} are the mean temperatures of the condenser and evaporator, A_p is the tube cross section area and U_{hp} is the global heat transfer coefficient calculated as in Chi (1976)

$$U_{hp} = \left[\frac{r_p^2 \ln(r_t / r_p)}{2L_e k_m} + \frac{r_p^2 \ln(r_p / r_v)}{2L_e k_{ef}} + \frac{\pi r_p^2 F_v \left(\frac{1}{6} L_e + L_a + \frac{1}{6} L_c \right) T_v}{\rho_v h_{fg}} + \frac{r_p^2 \ln(r_p / r_v)}{2L_c k_{ef}} + \frac{r_p^2 \ln(r_p / r_v)}{2L_c k_{ef}} \right]^{-1}$$

Where F_v is the friction coefficient for the vapor flow.

(ii) The energy balance in the condenser can be written as

$$Q_u = h_{cf} A_c (T_{tc} - T_f) \quad (36)$$

Where A_c is the condenser area and T_f is the mean temperature between the fluid at entry and exit.

(iii) Energy balance on the fluid results in

$$Q_u = \dot{m} C_p (T_{fs} - T_{fe}) \quad (37)$$

Eqs. (30), (31), (32), (35), (36) and (37) have six unknowns and therefore can be solved by Newton-Raphson method and the temperatures and the useful energy Q_u can be determined.

(iv) With this value of Q_u imposed as a boundary condition for the heat delivery to the evaporator one can solve the heat pipe model.

(v) In order to use the boundary condition of heat removal it is possible to represent the solution of Eq. (34) as below.

With the value of T_c as determined from the global formulation, considered as constant over the whole length of the condenser and discretizing Eq. (5) one can obtain

$$T_i = \left(1 - \frac{hP\Delta x}{\dot{m}C_p} \right) T_{i+1} + \frac{hP\Delta x}{\dot{m}C_p} T_m \quad (38)$$

(vi) This last equation which can be solved by a marching technique to obtain the temperature distribution in the fluid.

(vii) These values T_f are then used in the heat pipe model described earlier to obtain the temperature distribution along the heat pipe.

(viii) The new values of T_{ic} obtained in (vii) are used in Eq. (38) to obtain the new values of temperatures and the process is repeated until convergence is achieved.

(ix) The values of the temperatures T_{ie} are used in Eqs. (30), (31) and (32) to solve the system of equations corresponding to the evaporator (divided into N elements each of them of length Δz), by the method of Newton-Raphson. This process is repeated until all the temperature values are determined.

(x) Having determined these temperatures it is possible to calculate the efficiency of the system as

$$\eta = \frac{Q_u}{IWL_e} \quad \text{with} \quad Q_u = \sum_{i=1}^N Q_i \quad (39)$$

4. Experimental rig

To validate the proposed models of the heat pipe parabolic solar collector and the numerical predictions an experimental rig was designed, constructed and instrumented. The installation was used to heat up water for use in the Laboratory of Thermal Storage and Heat Pipes of the State University of Campinas, Brazil. The experimental system is shown in Fig. 4 and is composed of a single cylindrical parabolic solar concentrator of low concentration ratio (less than 5, 0), a constant head working fluid circulation circuit and a vacuum pump to produce vacuum into the glass envelop surrounding the heat pipe. The details of the experimental installation are shown in Fig. 4.

The parabolic mirror is supported by a bed hinged at both ends to allow the heat pipe collector system to be rotated for orientation and adjusting. The aperture angle of the collector is 90° , the focal distance is 10 cm, the length of the collector is 1 m and consequently the aperture area is 0.4 m^2 .

The absorber of the concentrator is a copper heat pipe painted black of 25.4 mm external diameter, with a wick made of bronze mesh sandwich. Water is used as the working fluid and its volume is 15 cm^3 . The heat pipe total length is 1.30 m, of which 1.0 m is the evaporator, 0.2 m is the condenser and 0.1 m is the adiabatic section length. The evaporator region is enveloped by a glass tube of 51 mm external diameter and 2 mm thickness with one of its ends fitted by end cap and reduced diameter connection to 10 mm to connect the glass envelop to the vacuum pump. A vacuum gauge is installed to measure the pressure in the annular space between the copper tube and glass envelop.

The thermocouples used are of the T-type of diameter 24 AWG. To be able to evaluate the heat pipe performance and the temperature distribution in the different sections along the heat pipe, the glass envelop and the rest of the system. Six thermocouples were placed in the evaporator region of which four thermocouples were placed in the middle of the evaporator spaced 90° along the perimeter of the of the heat pipe. One thermocouple was placed in the adiabatic region, two in the condenser region, one on the internal surface of the glass tube and one on its external surface. These thermocouples were calibrated against a certified thermometer of $\pm 0.05^\circ\text{C}$ precision. The

error propagation in the experimental work was evaluated using a conventional procedure. By using $\Delta T = \pm 0.05^\circ\text{C}$, $\Delta t = \pm 0.05$ s, volumetric error $\Delta V = \pm 0.1$ L the maximum error found in calculating the useful energy is found to be 6.7%.

General data and information relative to the experimental rig are listed below:

a. Reflector

- Reflectance $\rho_e = 0.7$
- Aperture area $A = 0.4 \text{ m}^2$

b. Heat Pipe

- Reflectance (visible) $\rho_{iv} = 0.03$
- Reflectance (infra-red) $\rho_{ii} = 0.10$
- Emittance (infra-red) $\varepsilon_i = 0.26$
- Evaporator length $L_e = 1.0$
- Condenser length $L_c = 0.2$ m
- Adiabatic length $L_a = 0.1$ m
- External diameter $d = 0.0254$ m

c. Glass Tube

- Transmittance (visible) $\tau_{vv} = 0.9$
- Reflectance (visible) $\rho_{vv} = 0.9$
- Transmittance (infra-red) $\tau_{vi} = 0.01$
- Reflectance (infra-red) $\rho_{vi} = 0.09$
- Emittance (infra-red) $\varepsilon_v = 0.9$
- Internal diameter $D_i = 0.047$ m
- External diameter $D_e = 0.050$ m

The tests were realized with the concentrator axis oriented along E-W direction at the city of Campinas, SP, Brazil.

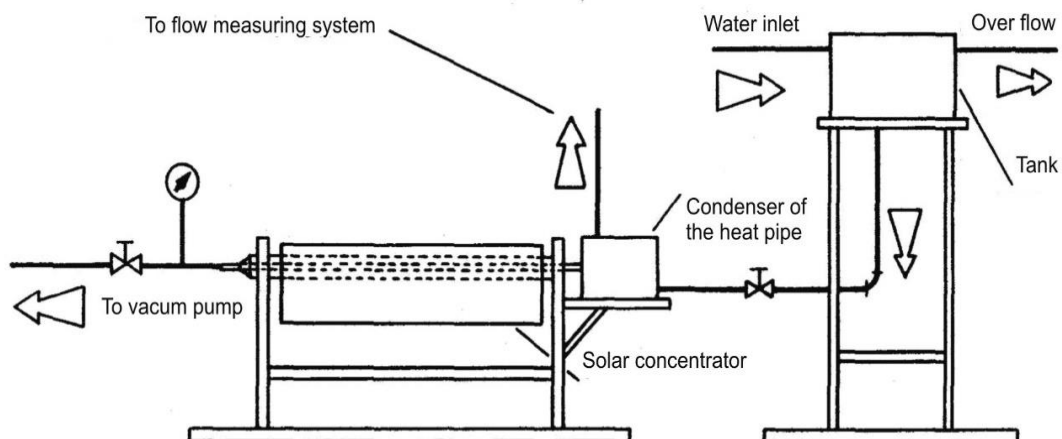


Fig. 4 Layout of the experimental apparatus

Testing procedure

With the concentrator axis oriented along E-W, the collector was rotated gently until the normal to the aperture area forms an angle γ corresponding to $\gamma=90-\beta$ with the horizontal, where β is the solar angle at mid solar day. After this adjustment is made, the collector is covered for protection while finalizing adjustments of the other components of the experimental rig. The pump for circulating water in the condenser of the heat pipe is switched on and the water flow rate is adjusted to the required value. The vacuum pump is connected to the collector evacuated tube, switched on and the vacuum is adjusted to a low value (10^{-5} mm Hg). All thermocouples are connected to the data acquisition system and finally to PC. The solar radiation was measured by Epply equipment and the continuous measurement evaluated at the end of each experiment. The local wind velocity is measured by digital anemometer and registered few times during each test.

With all the equipments adjusted the test is initiated and each 15 minutes all readings are collected automatically and the others are registered manually. In average three to four tests are done each hour. Most of the tests were realized between 10:30 and 14:30.

5. Results and discussion

Fig. 5 shows a comparison between the predictions from the present model and the results of Tien and Rohani (1972). As can be seen when the heat load is small the agreement between the present model predictions and the results of Tien and Rohani (1972) is good. When the heat load is increased the agreement is not as good. The differences can be attributed to the tolerances assumed in the numerical schemes adopted by Tien and Rohani (1972) and those adopted in the present study. Also since the temperature variation is big so will be the density variation and these will strongly affect the results. In their study they used the equation of perfect gas to correct the density while in the present work we interpolated values from gas tables.

The predicted results from the present model for the heat pipe were compared with the experimental results of McKinney (1969). The numerical simulations were realized under the same operational conditions as in McKinney's work (1969). Fig. 6 shows one of these comparative results indicating good agreement and consequently confirming the validity of numerical model. Other comparisons with McKinney's work showed good agreement and were omitted due to lack of space.

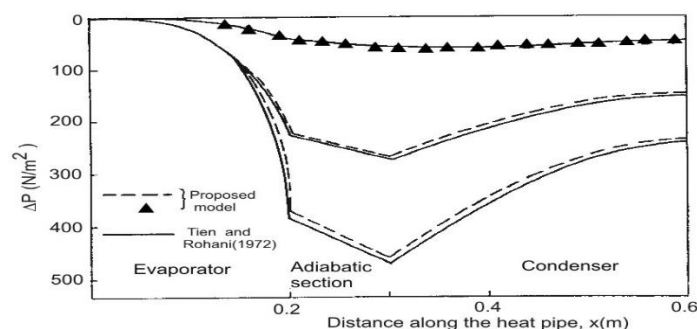


Fig. 5 Pressure drop in the heat pipe, comparison with the results of Tien and Rohani (1972)

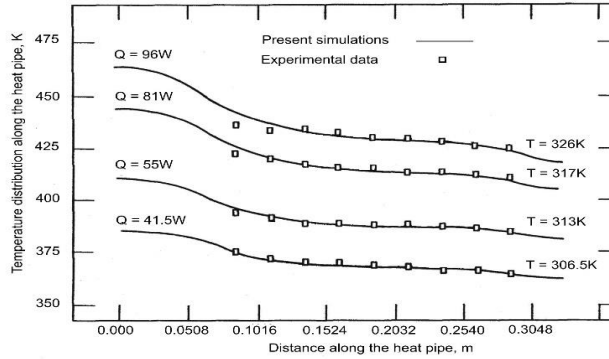


Fig. 6 Heat pipe temperature distribution, comparison with the results of Mc Kinney (1969)

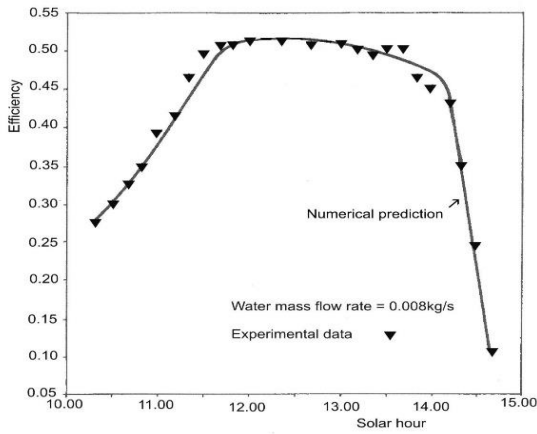


Fig. 7 Comparison between the hourly predicted efficiency and the experimental measurements

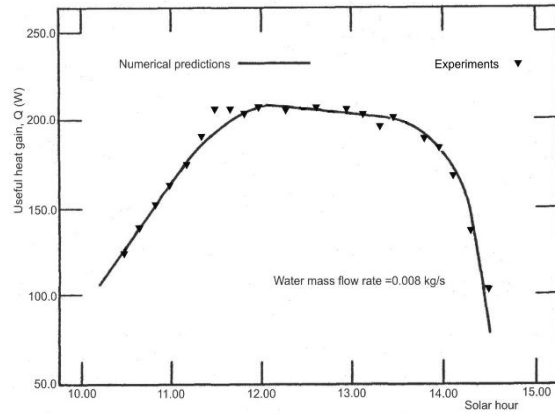


Fig. 8 Comparison between the numerical hourly heat gain and experimental measurements corresponding to the results of Fig. 7

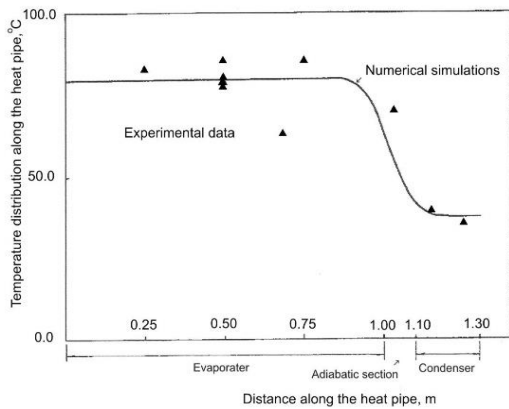


Fig. 9 Measured and predicted temperature distributions along the heat pipe corresponding to Figs. 7 and 8

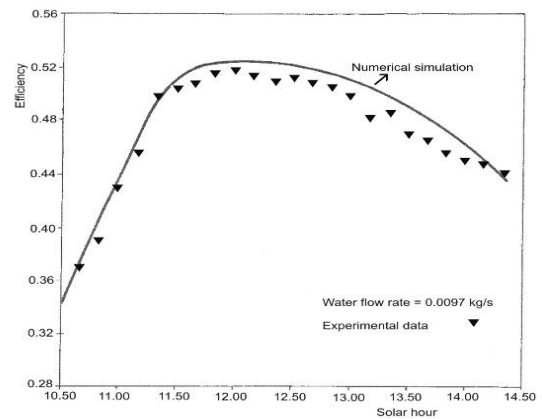


Fig. 10 Comparison between the predicted hourly efficiency and experimental measurements

As mentioned before the concentrator was oriented along the E-W direction. Fig. 7 shows a comparison between the daily experimental thermal efficiency and predicted numerical results. As can be seen the agreement is good. The corresponding variation of the useful energy rate with time for the same test is shown in Fig. 8 and as can be seen good agreement is found.

Fig. 9 shows the temperature distribution along the heat pipe corresponding to the results of Figs. 7 and 8. Because the heat received at the evaporator is not uniform, consequentially the circumferential temperature distribution is not uniform as can be verified from the experimental temperature distribution at mid section of the evaporator. At this location four thermocouples are fixed with angular spacing of 90° between them. As can be seen the higher temperature is indicated by the top thermocouple and the bottom thermocouple indicated the lowest temperature. The nearly coincident temperatures are indicated by the lateral thermocouples. This circumferential variation of the temperature distribution along the evaporator was not considered in the model. This assumption was adopted to avoid the complication of having to handle a three dimensional temperature profile in the heat pipe model. In the present study a uniform circumferential temperature distribution was adopted.

Fig. 10 shows the results of the hourly predicted thermal efficiency compared with the experimentally measured thermal efficiency. As can be seen the experimental values are below the predicted ones due to orientation errors since orientation is done manually. Fig. 11 shows the corresponding hourly heat gain for the results of Fig. 10 where the experimental measurements are slightly below the predicted ones due to orientation errors of the concentrator.

Fig. 12 shows the temperature distribution along the heat pipe corresponding to the results of Figs. 10 and 11. Again, because the heat received at the evaporator is not uniform, consequentially the circumferential temperature distribution is not uniform. This circumferential variation of the temperature distribution along the evaporator was not considered in the model to avoid having to handle a three dimensional temperature profile in the heat pipe model. For simplicity, in the present study a uniform circumferential temperature distribution was adopted.

Fig. 13 shows another comparison between the predicted hourly thermal efficiency and the

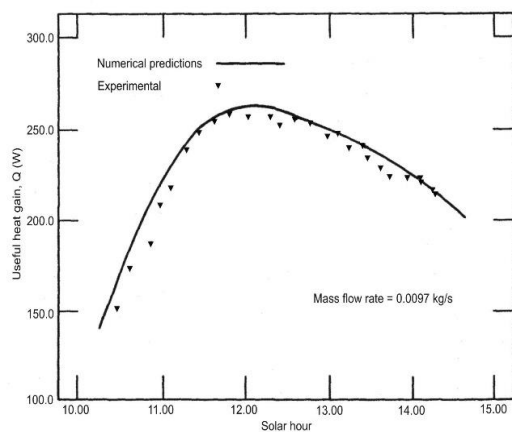


Fig. 11 Comparison between the numerical hourly useful heat gain and experimental measurements corresponding to the results of Fig. 10

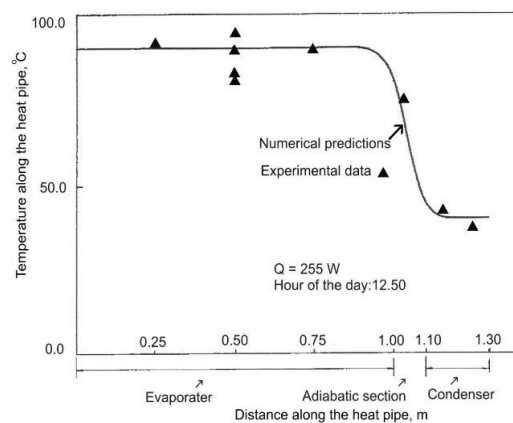


Fig. 12 Measured and predicted temperature distribution along the heat pipe corresponding to the results of Figs. 10 and 11

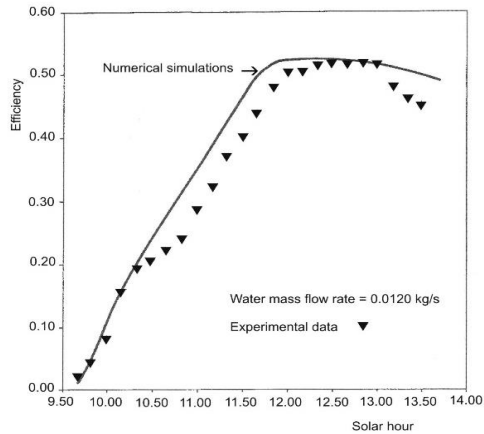


Fig. 13 Comparison between the numerical hourly efficiency and the experimental measurements

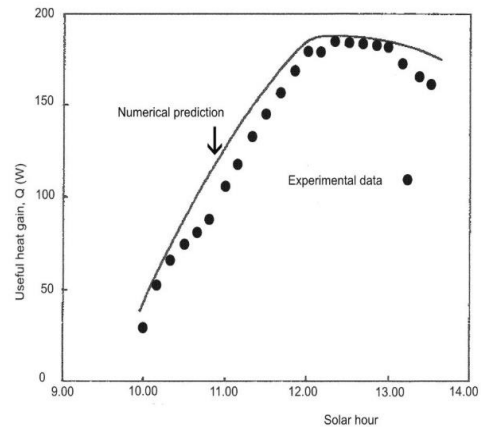


Fig. 14 Comparison between the numerical hourly useful heat gain and experiments corresponding to the results of Fig. 13

experimental measurements. The results show the same tendency as mentioned before. Fig. 14 shows the predicted useful heat gain and the experimental measurements corresponding to the results of Fig. 13. As can be verified there are some differences between the numerical predictions and measurements due to orientation errors.

6. Conclusions

The numerical predictions from the developed model of the copper heat pipe with porous wick are found to agree well with available experimental and numerical results. The validated model of the wicked heat pipe was inserted into evacuated glass tube and used as absorber for the cylindrical parabolic collector, the whole system was modeled and numerical simulations were realized with the concentrator oriented in the E-W direction, adjusted once a day. The numerical predictions were compared with experimental results showing acceptable agreement. The differences are attributed to orientation errors due to manual adjustment. An automatic tracking system can lead to better agreement.

Acknowledgments

The authors want to thank the CNPq for the PQ research scholarship to the first author and the pos-doctorate grant to the third author. Thanks are due the Capes for the doctorate scholarship to the second author.

References

Arab, M. and Abbas, A. (2013), "Model-based design and analysis of heat pipe working fluid for optimal

- performance in a concentric evacuated tube solar water heater”, *Sol. Energy*, **94**, 162-176.
- Ayompe, L.M. and Duffy, A. (2013), “Thermal performance analysis of a solar water heating system with heat pipe evacuated tube collector using data from a field trial”, *Sol. Energy*, **90**, 17-28.
- Azad, E. and Bahan, F. (1991), “The thermal performance of a co-axial heat pipe solar collector”, *J. Inst. Energy*, **64**, 107-112.
- Azad, E., Bahar, F. and Moztarzadeh, F. (1987), “Solar water heater using gravity assisted heat pipe”, *Heat Recov. Syst. CHP*, **7**(4), 343-350.
- Biencinto, M., González, L. and Valenzuela, L. (2016), “A quasi-dynamic simulation model for direct steam generation in parabolic troughs using TRNSYS”, *Appl. Energy*, **161**, 133-142.
- Cabrera, F.J., Fernandez-Garcia, A., Silva, R.M.P. and Perez-Garcia, M. (2013), “Use of parabolic trough solar collectors for solar refrigeration and air-conditioning applications”, *Renew. Sustain. Energy Rev.*, **20**, 103-118.
- Chi, S.W. (1976), *Heat Pipe-Theory and Practice: A Source Book*, Hemisphere Publishing Corporation.
- Chong, K.K., Chay, K.G. and Chin, K.H. (2012), “Study of a solar water heater using stationary v-trough collector”, *Renew. Energy*, **39**(1), 207-215.
- Chun, W., Kang, Y.H., Kwak, H.Y. and Lee, Y.S. (1999), “An experimental study of the utilization of heat pipes for solar water heaters”, *Appl. Therm. Eng.*, **19**(8), 807-817.
- Conrado, L.S., Rodríguez-Pulido, A. and Calderón, G. (2017), “Thermal performance of parabolic trough solar collectors”, *Renew. Sustain. Energy Rev.*, **67**, 1345-1359.
- Duffie, J.A. and Beckman, W.A. (2013), “Solar engineering of thermal processes”, *Renew. Sustain. Energy Rev.*, **54**, 1085-1091.
- Gari, H.A. and Fathalah, K.A. (1988), “Modeling and simulation of a passive condensate heat pipe pumping system for solar energy applications”, *Heat Recov. Syst. CHP*, **8**(6), 559-569.
- Ghaddar, N. and Nasr, Y. (1998), “Experimental study of a refrigerant charged solar collector”, *J. Energy Res.*, **22**, 625-638.
- Guo, J., Huai, X. and Liu, Z. (2016), “Performance investigation of parabolic trough solar receiver”, *Appl. Therm. Eng.*, **95**, 357-364.
- Hachicha, A.A., Rodríguez, I., Capdevila, R. and Oliva, A. (2013), “Heat transfer analysis and numerical simulation of a parabolic trough solar collector”, *Appl. Energy*, **111**, 581-592.
- Hussein, H.M.S., Mohamad, M.A. and El-Asfour, A.S. (1999), “Optimization of a wickless heat pipe flat plate solar collector”, *Energy Convers. Manage.*, **40**(18), 1949-1961.
- Ismail, K.A.R. and Zanardi, M.A. (1990), “Cylindrical parabolic solar collector with heat pipe absorber”, *Proceedings of the World Renewable Energy Congress*, Reading, UK, **2**, 1242-1246.
- Ismail, K.A.R. and Zanardi, M.A. (1993), “Experimental verification of a two-dimensional model for porous wick heat pipes”, *Proceedings of the III World Conference on Experimental Heat Transfer, Fluid Mechan. Thermodyn.*, Honolulu, Hawaii, 427-432.
- Jebasingh, V.K. and Herbert, G.M.J. (2016), *A Review of Solar Parabolic Trough Collector*, 4th Edition, John Wiley & Sons, Inc.
- Kim, Y. and Seo, T. (2007), “Thermal performances comparisons of the glass evacuated tube solar collectors with shapes of absorber tube”, *Renew. Energy*, **32**(5), 772-795.
- Kreith, F., Manglik, R.M. and Bohn, M.S. (2011), *Principles of Heat Transfer*, 7th Edition, Cengage Learning Inc.
- Kumar, K.R. and Reddy, K.S. (2009), “Thermal analysis of solar parabolic trough with porous disc receiver”, *Appl. Energy*, **86**(9), 1804-1812.
- Liang, H., You, S. and Zhang, H. (2015), “Comparison of different heat transfer models for parabolic trough solar collectors”, *Appl. Energy*, **148**, 105-114.
- McAdams, W.J. (1954), *Heat Transmission*, 3rd Edition, McGraw Hill.
- McKinney, B.G. (1969), “An experimental and analytical study of water heat pipes for moderate temperature ranges”, *NASA TM-53849*.
- Nkwetta, D.N., Smyth, M., Zacharopoulos, A. and Hyde, T. (2012), “In-door experimental analysis of concentrated and non-concentrated evacuated tube heat pipe collectors for medium temperature

- applications”, *Energy Build.*, **47**, 674-681.
- Ortobasi, U. and Buehl, W.M. (1980), “An internal cusp reflector for an evacuated tubular heat pipe solar thermal collector”, *Sol. Energy*, **25**(1), 67-78.
- Padilla, R.V., Demirkaya, G., Goswami, D.Y., Stefanakos, E. and Rahman, M.M. (2011), “Heat transfer analysis of parabolic trough solar receiver”, *Appl. Energy*, **88**(12), 5097-5110.
- Ramsey, J.W., Gupta, B.P. and Knowles, G.R. (1977), “Experimental evaluation of a cylindrical parabolic solar collector”, *J. Heat Transf.*, **99**(2), 163-168.
- Ratzel, A.C., Hickox, C.E. and Gartling, D.K. (1979), “Techniques for reducing thermal conduction and natural convection heat losses in annular receiver geometries”, *J. Heat Transf.*, **101**(1), 108-113.
- Redpath, D.A.G., Eames, P.C., Lo, S.N.G. and Griffiths, P.W. (2009), “Experimental investigation of natural convection heat exchange within a physical model of the manifold chamber of a thermo-syphon heat pipe evacuated tube solar water heater”, *Sol. Energy*, **83**(7), 988-997.
- Tien, C.L. and Rohani, R. (1972), “Theory of two component heat pipe”, *J. Heat Transf.*, **94**(4), 479-484.
- Umarov, G.I., Zakhidov, R.A. and Khodzhaev, A.S. (1976), “Radiant vector distribution in the radiant field of a parabolic cylindrical concentrator”, *Geliotekhnika*, **12**, 27-32.
- Vafai, K. and Tien, C.L. (1981), “Boundary and inertia effects on flow and heat transfer in porous media”, *J. Heat Mass Transf.*, **24**(2), 195-203.
- Vasiliev, L.L., Grakovich, L.P. and Khrustaler, D.K. (1984), “Optimization of flat plate solar energy heat pipe collector parameters”, *Heat Recov. Syst. CHP*, **1**(3), 157-164.
- Wang, Y., Zhu, Y., Chen, H., Zhang, X., Yang, L. and Liao, C. (2015), “Performance analysis of a novel sun-tracking CPC heat pipe evacuated tubular collector”, *Appl. Therm. Eng.*, **87**, 381-388.
- Wong, H.H. and Raithby, G.D. (1979), “Improved finite difference methods based on critical evaluation of the approximation errors”, *Numer. Heat Transf.*, **2**(2), 139-163.
- Zou, B., Dong, J., Yao, Y. and Jiang, Y. (2016), “An experimental investigation on a small-sized parabolic trough solar collector for water heating in cold areas”, *Appl. Energy*, **163**, 396-407.

CC

Nomenclature

A	Aperture area
A_p	Tube cross sectional area
c_p	Specific heat ($\text{J kg}^{-1} \text{K}^{-1}$)
D, d	Diameter (m)
Dar	Darcy number $= \frac{r_v^2 \varepsilon}{K}$
$F(\alpha)$	Correction factor
g	Gravitational acceleration (m s^{-2})
H	Heat transfer coefficient ($\text{W m}^{-2} \text{K}^{-1}$)
λ	Latent heat of vaporization (J kg^{-1})
I	Solar radiation intensity (W m^{-2})
K	Permeability of porous medium
K	Thermal conductivity ($\text{W m}^{-1} \text{K}^{-1}$)
L	Length (m)
\dot{m}	Mass flow (kg s^{-1})
n	Day of the year

Greek Symbols

α	Diffusivity ($\text{m}^2 \text{s}^{-1}$)
β	Solar height
γ	Azimuth angle
ϕ	Latitude angle
δ	Sun declination angle
ε	Emittance, porosity
θ	Incidence angle
μ	Dynamic viscosity ($\text{kg s}^{-1} \text{m}^{-1}$)
ν	Kinematic viscosity ($\text{m}^2 \text{s}^{-1}$)
ρ	Density (kg m^{-3}) or reflectance
σ	Stefan-Boltzmann constant
τ	Transmittance
ω	Hourly angle
λ	Vaporization Latent heat (J kg^{-1})

Nomenclature

P	Perimeter (m)
Pr	Prandtl number $= \frac{\mu_{vr} c_{pv}}{k_v}$
Pr_p	Prandtl number in the porous material $= \frac{\mu_{vr} c_{pl}}{k_{eff}}$
P	Pressure (N m ⁻²)
Q	Power (W)
Ra	Rayleigh number defined as $Ra = \rho g \beta l^3 \frac{\Delta T}{\mu \alpha}$
Re_r	Radial Reynolds number
R	Radial coordinate, radius (m)
S	Inclination angle (rad.)
T	Temperature (K)
U	Heat transfer coefficient (W m ⁻² K ⁻¹)
U	Axial velocity (m s ⁻¹)
V	Radial velocity (m s ⁻¹)
W	Collector width (m)
X	Axial coordinate
Y	Interception factor
Re_{rp}	Radial Reynolds number in the porous material

Subscripts and Superscripts

A	Adiabatic region, ambient
c	Condenser
e	Evaporator, external
eff	Effective
ef	For equation (25a)
f_s	Exit
f_e	Entry
i	Internal
L	Liquid
m	Metallic
p	Porous medium
r	Reference
tc	Heat pipe
t	Tube
ti	Tube in the infrared range
tv	Glass tube
v	Vapor, glass
vi	Glass in the infrared range
vv	Glass in the visible range
*	Dimensionless value
vr	Vapor phase in the radial direction